PHYSICAL REVIEW B **72**, 184426 (2005)

High-temperature orbital, charge, and structural phase transitions in the cation-ordered manganites $TbBaMn_2O_6$ and $YBaMn_2O_6$

Anthony J. Williams and J. Paul Attfield
Centre for Science at Extreme Conditions, University of Edinburgh, Erskine Williamson Building, King's Buildings, Mayfield Road, Edinburgh EH9 3JZ, United Kingdom

Simon A. T. Redfern
Department of Earth Sciences, University of Cambridge, Downing Street, Cambridge CB2 3EQ, United Kingdom

(Received 23 June 2005; revised manuscript received 29 August 2005; published 22 November 2005)

The high-temperature structures and phase transitions of the cation-ordered manganite perovskites $TbBaMn_2O_6$ and $YBaMn_2O_6$ have been studied by powder neutron diffraction and differential scanning calorimetry. $TbBaMn_2O_6$ undergoes an unprecedented transition from a charge and antiferro-orbitally ordered phase to a charge and ferro-orbitally ordered structure at 94.5 °C, and the charge and orbital ordering melts at 200 °C. An orthorhombic *Cmmm* phase with rotational order of MnO_6 octahedra is observed above the transition, and at 514 °C this transforms to the aristotype tetragonal $P4/mmm$ arrangement. $YBaMn_2O_6$ is charge and ferro-orbitally ordered up to 225 °C. Above this charge ordering transition, a $C2/m$ phase with two rotational orders is found. This transforms to the *Cmmm* structure at 437 °C. Discontinuities in volume and volume expansion, and a limited phase coexistence region are observed at the charge ordering transitions, whereas the other transitions are continuous.

DOI: 10.1103/PhysRevB.72.184426 PACS number(s): 75.47.Lx, 64.70.Kb, 71.30.+h, 61.12.Ld

I. INTRODUCTION

Manganese oxide perovskites with the general formula $Ln_{1-x}M_xMnO_3$ (Ln=trivalent lanthanide, M=Ca, Sr, or Ba) have attracted considerable attention over the past decade on account of their unusual magnetic and electronic properties—most notably the phenomenon of colossal magnetoresistance. They exhibit a very rich phase diagram with a wide variety of magnetic and electronic states that can be interconverted by chemical changes at the perovskite A site.

More recently, a series of 50% doped manganites, $RBaMn_2O_6$, has been studied,[1–5] in which the R^{3+} and Ba^{2+} cations are ordered in alternating [001] perovskite layers. For large R=Nd—La, a ferromagnetic metallic state is observed, but with higher Curie temperatures than in cation-disordered analogs (for example, for $LaBaMn_2O_6$,[1] T_c increases from 270 to 335 K). At lower temperatures, the ferromagnetic phase transforms to an A-type antiferromagnetic structure in $NdBaMn_2O_6$ and $PrBaMn_2O_6$,[3] but the crystal structure remains tetragonal with no charge or orbital ordering distortions observed at any temperature. For small R=Y, Sm—Ho, however, the internal strains imposed by the A-cation ordering of mismatched layers leads to the stabilization of novel charge and orbitally ordered structures.

Room temperature studies of the A-cation ordered manganites $TbBaMn_2O_6$ (Ref. 6) and $YBaMn_2O_6$ (Ref. 7) showed them to each adopt novel ground state structures. $TbBaMn_2O_6$ was shown by neutron diffraction to have a highly distorted triclinic $\sqrt{2}a_p \times 2\sqrt{2}a_p \times 2a_p$ perovskite superstructure at 300 K which, in addition to the long-range ordering of Tb^{3+} and Ba^{2+}, exhibits a long-range ordering of Mn^{3+} and Mn^{4+} charge states and Mn^{3+} orbital states. The charge order (CO) is of the "rock salt" type, and not the "striped" arrangement found in conventional half-doped manganites such as $(La_{0.5}Ca_{0.5})MnO_3$.[8] Antiferro-orbital order (AFOO) of the Mn^{3+} Jahn-Teller distortions is observed, with the orbital distortions of successive Mn^{3+} sites in the *b*-direction being mutually perpendicular. $YBaMn_2O_6$ also has a distorted triclinic superstructure $(\sqrt{2}a_p \times \sqrt{2}a_p \times 2a_p)$ with the same "rocksalt" charge ordering, but with a ferro-type orbital ordering (FOO), in which adjacent d_{z_2}-type orbitals are parallel so that the *b*-axis periodicity does not double.

In the present publication, we report the results of high-temperature neutron diffraction studies carried out on $TbBaMn_2O_6$ and $YBaMn_2O_6$ to determine the thermal evolution of the long-range orderings observed in these materials and to study the structural changes at the associated phase transitions.

II. EXPERIMENT

The samples are the same as were used in room-temperature diffraction studies and their syntheses have been reported previously.[6,7] Powder neutron diffraction data were collected from the HRPD instrument at the ISIS facility, United Kingdom, at temperatures between 14 and 600 °C for $TbBaMn_2O_6$ and between 14 and 500 °C for $YBaMn_2O_6$. Profiles from the backscattering $(2\theta=168°)$ and the $2\theta=90°$ detector banks were Rietveld analyzed using the General Structure Analysis System (GSAS) program.[9] The backscattering detector bank gives extremely high *d*-space resolution $(\Delta d/d=4\times10^{-4})$ which proved essential for determining the subtle superstructures of these phases. No loss of oxygen at high temperatures was evident from either sample through refinement of oxygen site occupation factors. However, a recent thermogravimetric study found that $YBaMn_2O_6$ loses oxygen above 400 °C under a reducing atmosphere, with a 2% loss up to 600 °C,[10] so the results for temperatures >400 °C may be influenced slightly by a small oxygen deficiency.

Differential scanning calorimetry (DSC) measurements were made on $TbBaMn_2O_6$ using a Perkin Elmer Pyris-Diamond DSC at the University of Cambridge, Department of Earth Sciences. With this instrument, a small low-mass furnace allows rapid heating, cooling, and equilibration for small (<100 mg) samples. Calorimetry is conducted via power compensation. Both rapid heating and step scan analyses were employed. The former was used at relatively high heating rates (20 °C/min), which were required to pick up the small heat effect at the subtle and continuous (second-order) orbital ordering transition suspected between room temperature and 100 °C. The step scan measurements, with an effective heating rate of approximately 1.5 °C/min under a 20 ml/min flow of N_2, were made between 120 and 260 °C to study the charge ordering transition which was known to be first-order in character. Three temperature regions, covering the major transitions identified in the neutron diffraction data, were independently probed −65 to 120 °C, 120 to 260 °C, and 525 to 555 °C. Calorimetry data collected over the last of these temperature regions suffered from high noise and a less stable baseline, and were not of sufficient quality to reveal any effect due to a phase transition above the noise.

III. $TbBaMn_2O_6$

A. Phase transitions

The room temperature diffraction profile of $TbBaMn_2O_6$, as described in Ref. 6, is characterized by a series of superstructure reflections and peak splittings. Charge order is evidenced by a monoclinic symmetry distortion of the tetragonal $RBaMn_2O_6$ cell, and the antiferro-orbital order gives rise to weak $(h\frac{k}{2}l)$ superstructure reflections such as $(2\frac{1}{2}0)$and $(1\frac{3}{2}1)$ that evidence a *b*-doubled AFOO superstructure.

At 100 °C, the lowest temperature here investigated, the *b*-doubled superstructure reflections were not observed. The major, monoclinic $P2_1/m$ superstructure reflections, most noticeable at around 2.30 and 2.35 Å, are still present, however, and the intense (202) reflection remains split. A similar pattern of reflections was observed at all temperatures up to 175 °C.

The pattern changes around 200 °C (Fig. 1), above which the monoclinic splitting of the intense (202) peak is no longer observed, and several superstructure reflections such as (211) disappear. The retention of other superstructure peaks such as the (103) reflection at ~2.3 Å show that the symmetry is still lower than the aristotype tetragonal $P4/mmm$ symmetry. Lowering the symmetry from the tetragonal model to the orthorhombic space group $Cmmm$, in which all Mn sites are equivalent, generates all the observed superstructure reflections. This space group is also consistent with the group theoretical analysis for layered ordering on the perovskite A site conducted by Howard and Zhang,[11] and similarly observed for the layered titanate perovskite, $La_{2/3}TiO_3$. The 200 °C pattern shows a clear phase coexistence, with reflections characteristic of both the orthorhombic $Cmmm$ and monoclinic $P2_1/m$ phases being observed.

Above 500 °C, all superstructure peaks are absent. The observed reflections can be indexed on an aristotype $P4/mmm$ symmetry, $LaBaMn_2O_6$-type cell.

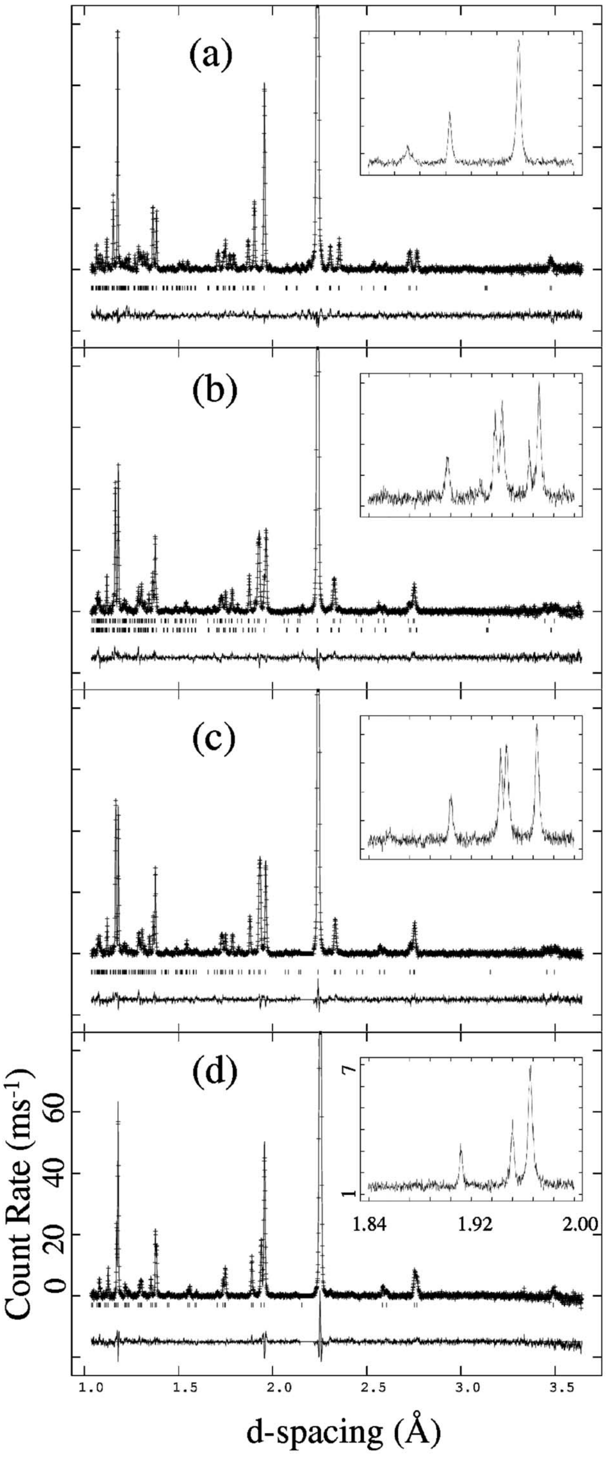

FIG. 1. Powder neutron diffraction profiles from the $2\theta=90°$ HRPD detector for $TbBaMn_2O_6$ at representative temperatures. (a) 100 °C fitted in monoclinic space group $P2_1/m$. (b) 200 °C fitted as a mixture of monoclinic $P2_1/m$ and orthorhombic $Cmmm$ phases. (c) 300 °C fitted in orthorhombic spacegroup $Cmmm$. (d) 600 °C fitted in tetragonal spacegroup $P4/mmm$. The intense (202) reflection at 2.2 Å has a peak count rate of 330 ms^{-1}, but the vertical scale has been truncated to enable other peaks to be seen clearly. The inset regions show the sensitivity of the backscattering detector data to the changes of symmetry and phase coexistence in (b).

TABLE I. Refined structural models for representative $RBaMn_2O_6$ phases.

	Atom	Site	x	y	z	U_{iso}(Å^2)
$TbBaMn_2O_6$	Tb	2e	0.7243(5)	0.25	0.5052(5)	0.0077(3)
Temperature: 100 °C	Ba	2e	0.7741(8)	0.25	−0.0020(7)	0.0077(3)
Space group: $P2_1/m$	Mn(1)	2e	0.2418(10)	0.25	0.2480(7)	0.0073(10)
	Mn(2)	2e	0.2513(10)	0.25	−0.2636(7)	0.0040(12)
	O(1)	4f	0.4955(5)	0.4748(5)	0.2563(2)	0.0127(6)
	O(2)	2e	0.2491(7)	0.25	−0.0068(6)	0.0112(6)
	O(3)	2e	0.2180(8)	0.25	0.5109(7)	0.0423(10)
	O(4)	4f	−0.0058(6)	0.0071(5)	0.2942(2)	0.0033(5)
$TbBaMn_2O_6$	Tb	4h	0.2250(2)	0	0.5	0.0056(2)
Temperature: 225 °C	Ba	4g	0.2677(4)	0	0	0.0056(2)
Space group: $Cmmm$	Mn	8n	0	0.2513(5)	0.2555(2)	0.0011(4)
	O(1)	4j	0	0.2339(5)	0.5	0.0520(9)
	O(2)	4i	0	0.2508(5)	0	0.0149(7)
	O(3)	4l	0	0.5	0.3003(2)	0.0042(6)
	O(4)	4k	0	0	0.2477(3)	0.0011(6)
	O(5)	8m	0.25	0.25	0.2797(2)	0.0150(5)
$YBaMn_2O_6$	Y	4i	0.2363(2)	0	0.4948(2)	0.0129(2)
Temperature: 250 °C	Ba	4i	0.2521(4)	0	−0.0040(5)	0.0129(2)
Space group: $C2/m$	Mn	8j	0.0004(4)	0.2479(3)	0.2554(2)	0.0027(3)
	O(1)	4h	0	0.2058(3)	0.5	0.0219(7)
	O(2)	4g	0	0.2690(3)	0	0.0092(6)
	O(3)	4i	−0.0159(3)	0.5	0.2993(3)	0.0104(6)
	O(4)	4i	0.0250(3)	0	0.2503(2)	0.0202(7)
	O(5)	8j	0.2450(3)	0.2678(2)	0.2789(1)	0.0191(3)

B. Structural models

1. $P2_1/m$ (or $P\bar{1}$) phase

Over the 100–175 °C temperature range, the diffraction profile of $TbBaMn_2O_6$ is almost identical to the room temperature profile of $YBaMn_2O_6$ (Ref. 7). The diffraction patterns of both materials can be described by a monoclinic $P2_1/m$ model in which no Mn^{3+} orbital ordering distortions in the ab-plane are present. However, for $YBaMn_2O_6$, the partly resolved splitting of some reflections, e.g., the (220) peak, evidenced a lowering of symmetry to triclinic $P\bar{1}$ that results from ferro-orbital ordering.[7]

The 100–175 °C $TbBaMn_2O_6$ structures were refined in the monoclinic space group $P2_1/m$ (a representative structural model is shown in Table I) and this gave a good fit to the data at all temperatures [see Table II for all lattice parameters and Fig. 1(a)]. This symmetry model cannot describe Mn^{3+} orbital ordering distortions in the ab-plane, as verified by the Mn—O distances in Table III, although distortions of the MnO_6 polyhedra due to structural strains are observed. The difference between the mean Mn—O distances of the two distinct manganese sites, however, remains significant, confirming that the Mn^{3+}/Mn^{4+} "rock salt" type charge ordering is maintained in this phase (Fig. 2).

Refinement of the FOO triclinic $P\bar{1}$ model was also attempted for the 100 °C $TbBaMn_2O_6$ pattern to compare the two models. However, no triclinic splittings or broadenings were observable in this pattern, and free refinement of the $P\bar{1}$ model was unstable. Constraining the x and y displacements of pairs of O1 and O4 sites to mimic the FOO observed in $YBaMn_2O_6$ allowed a free refinement of all other parameters, and a marginally but not significantly improved fit was obtained ($\chi^2=4.94$, $R_{wp}=4.87\%$) over the $P2_1/m$ model ($\chi^2=5.38$, $R_{wp}=5.08\%$)

Two possibilities are thus apparent for the 100–175 °C phase of $TbBaMn_2O_6$. If the symmetry is genuinely $P2_1/m$ then the phase is charge ordered but orbitally disordered; the Mn^{3+} Jahn-Teller distortions are present locally, but are spatially incoherent over long distances. In this case the structural transition between room temperature and 100 °C corresponds to an orbital order (AFOO) to disorder transition. Alternatively, the phase may be triclinic $P\bar{1}$ with charge ordering and ferro-orbital ordering. The peak broadenings which evidenced this descent to triclinic symmetry in $YBaMn_2O_6$ were extremely subtle, and it is possible that they are also present in $TbBaMn_2O_6$ but are below the resolution of the HRPD instrument. In this case, the transition between room temperature and 100 °C in $TbBaMn_2O_6$

TABLE II. Thermal evolution of the space group symmetry and lattice parameters of $TbBaMn_2O_6$.

Temperature (°C)	Space group	*a* (Å)	*b* (Å)	*c* (Å)	β (°)
100	$P2_1/m$	5.53033(7)	5.53086(7)	7.60836(7)	90.195(1)
125	$P2_1/m$	5.53073(7)	5.53133(7)	7.61379(7)	90.177(1)
150	$P2_1/m$	5.52976(8)	5.53159(8)	7.61837(7)	90.156(1)
175	$P2_1/m$	5.52783(9)	5.53009(9)	7.62507(7)	90.134(1)
200	$P2_1/m$	5.53075(5)	5.52582(4)	7.63210(2)	90.134(6)
200	*Cmmm*	7.71274(10)	7.85532(9)	7.68470(9)	
225	*Cmmm*	7.71851(8)	7.85554(8)	7.69249(8)	
250	*Cmmm*	7.72321(7)	7.85372(8)	7.69770(7)	
275	*Cmmm*	7.72793(7)	7.85157(8)	7.70282(7)	
300	*Cmmm*	7.73277(7)	7.84927(8)	7.70718(7)	
350	*Cmmm*	7.74381(7)	7.84487(8)	7.71736(7)	
400	*Cmmm*	7.75624(7)	7.83936(8)	7.72651(7)	
450	*Cmmm*	7.77108(8)	7.83319(9)	7.73605(8)	
500	*Cmmm*	7.7904(9)	7.82192(9)	7.74538(9)	
550	$P4/mmm$	3.90562(4)	3.90562(4)	7.74983(8)	
600	$P4/mmm$	3.91094(4)	3.91094(4)	7.75141(8)	

would represent a AFOO to FOO transition within the CO regime. The two possibilities cannot be distinguished from the neutron structure refinements, but the latter interpretation is favored by DSC data as described later.

2. *Cmmm* phase

At temperatures between 225 and 500 °C, the profile was fitted in orthorhombic space group *Cmmm* (Table I). A good

TABLE III. Manganese-oxygen distances (Å) in the structural phases of $TbBaMn_2O_6$. Two Mn sites are observed in the CO region below 200 °C, but only one site is found at higher temperatures.

		Mn1-O				Mn2-O					
Temperature (°C)	Space group	Mn1-O1 (×2)	Mn1-O2	Mn1-O3	Mn1-O4 (×2)	Mn2-O1 (×2)	Mn2-O2	Mn2-O3	Mn2-O4 (×2)	⟨Mn1-O⟩	⟨Mn2-O⟩
100	$P2_1/m$	1.991(6)	1.888(8)	1.946(8)	2.006(5)	1.935(5)	2.012(8)	1.841(7)	1.940(5)	1.971(7)	1.934(7)
125	$P2_1/m$	1.987(7)	1.899(9)	1.940(8)	2.016(5)	1.921(5)	1.992(8)	1.856(7)	1.948(5)	1.974(7)	1.931(7)
150	$P2_1/m$	1.979(6)	1.887(7)	1.952(8)	1.995(5)	1.935(5)	2.007(8)	1.840(7)	1.966(5)	1.965(7)	1.942(7)
175	$P2_1/m$	1.987(9)	1.888(9)	1.954(8)	2.002(7)	1.923(7)	2.009(8)	1.842(8)	1.956(6)	1.970(7)	1.935(7)
				Mn—O							
		Mn—O1	Mn—O2	Mn—O3	Mn—O4	Mn—O5 (×2)				⟨Mn—O⟩	
225	*Cmmm*	1.886(2)	1.965(2)	1.984(4)	1.975(4)	1.939(2)				1.948(1)	
250	*Cmmm*	1.887(2)	1.965(2)	1.998(4)	1.960(4)	1.941(2)				1.949(1)	
275	*Cmmm*	1.889(2)	1.966(2)	1.990(4)	1.967(4)	1.941(2)				1.949(1)	
300	*Cmmm*	1.893(2)	1.967(2)	1.978(4)	1.976(4)	1.942(2)				1.950(1)	
350	*Cmmm*	1.897(2)	1.967(2)	1.989(4)	1.962(4)	1.945(2)				1.951(1)	
400	*Cmmm*	1.903(2)	1.966(2)	1.979(4)	1.967(4)	1.949(2)				1.952(1)	
450	*Cmmm*	1.901(2)	1.973(2)	1.977(4)	1.961(4)	1.952(2)				1.953(1)	
500	*Cmmm*	1.907(2)	1.976(2)	1.964(4)	1.965(4)	1.955(3)				1.954(1)	
		Mn—O1 (×4)		Mn—O2		Mn—O3					
550	$P4/mmm$	1.959(2)		1.980(2)		1.895(2)				1.952(1)	
600	$P4/mmm$	1.963(2)		1.979(2)		1.897(2)				1.955(1)	

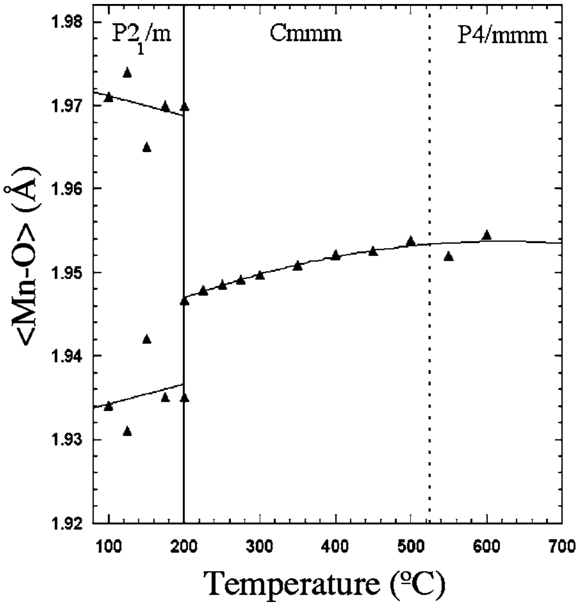

FIG. 2. Temperature dependence of the average Mn—O bond lengths in $TbBaMn_2O_6$. Lower temperature $P2_1/m$ structures contain two manganese sites, higher temperature structures only one. Solid/dashed vertical lines show the first/second-order phase transitions. Lines through points are guides to the eye.

fit was obtained for all patterns [Table II; Fig. 1(c)]. All manganese sites are equivalent, with a mean Mn—O distance intermediate between the Mn^{3+} and Mn^{4+}—O distances observed in the charge ordered monoclinic phase, and no significant orbital ordering distortion is seen although the MnO_6 octahedra remain irregular. The structure has neither charge nor orbital long range order. The *Cmmm* to $P2_1/m$ (or $P\bar{1}$) transition at 200 °C is therefore the charge ordering transition (T_{CO}) in $TbBaMn_2O_6$.

3. *P*4/*mmm* phase

Above 500 °C, all patterns were well-fitted by the $P4/mmm$ aristotype structure [Fig. 1(d)] in which there is only one manganese site. The Tb and Ba cation layers on either side of each MnO_6 polyhedron create a local polar distortion with long Mn—O2 and short Mn—O3 bonds in the ±*c* directions. Independent refinement of the fractional occupancies of the Tb and Ba sites at these temperatures showed no antisite disorder to an experimental uncertainty of 2.5%. The structure is neither charge nor orbitally ordered.

C. Critical variations

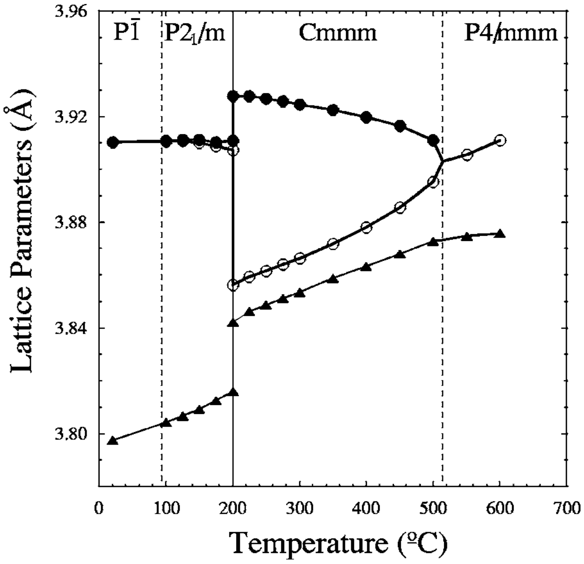

FIG. 3. Temperature dependence of the pseudo-cubic *a* (closed circles), *b* (open circles), and *c* (triangles) lattice parameters of $TbBaMn_2O_6$, Solid/dashed vertical lines show the first/second-order phase transitions.

The refined cell parameters, and cell volume of $TbBaMn_2O_6$ (Figs. 3 and 4, Table II), show steady increases with temperature. There is, however, a strong discontinuity at the 200 °C charge ordering transition, as well as a marked change in the slope of the cell volume ($\Delta V/V = 1.65 \times 10^{-3}$ in the monoclinic regime versus 4.28×10^{-3} in the orthorhombic). The discontinuity in the cell parameters, coupled with the phase coexistence observed at the charge ordering transition are clearly indicative of it being first order, whereas the continuous variation of the cell parameters through the *Cmmm* to $P4/mmm$ transition strongly suggest it to be second order.

The macroscopic strains in the high temperature *Cmmm* structure can be characterized by an orthorhombic distortion of the tetragonal unit cell, which can be approximated as the orthorhombic spontaneous strain, $o = 2(b-a)/(b+a)$. Landau's theory of second-order phase transitions predicts that order parameters, Q, should be proportional to $(1-T/T_0)^{\beta}$, for temperatures below the transition temperature T_0, with β taking values of $1/2$ for second-order phase transitions and $1/4$ for a tricritical phase transition. The *Cmmm*-$P4/mmm$ symmetry change involves a doubling of the unit cell along *x* and *y* (a quadrupling of the cell volume) on transformation to

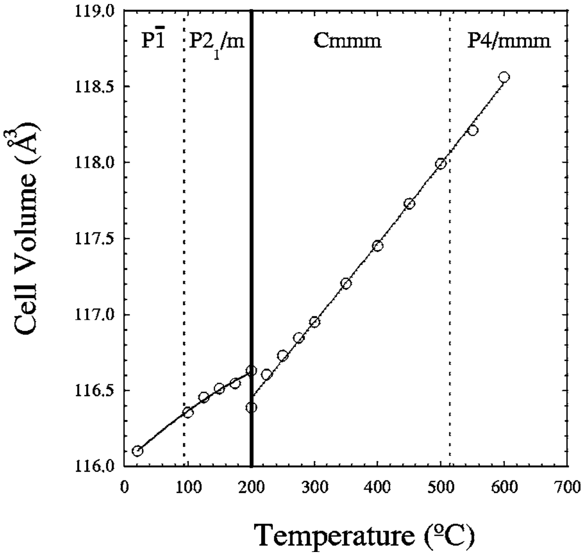

FIG. 4. Temperature dependence of cell volume of $TbBaMn_2O_6$. Solid/dashed vertical lines show the first/second-order phase transitions. Lines through points are a guide to the eye.

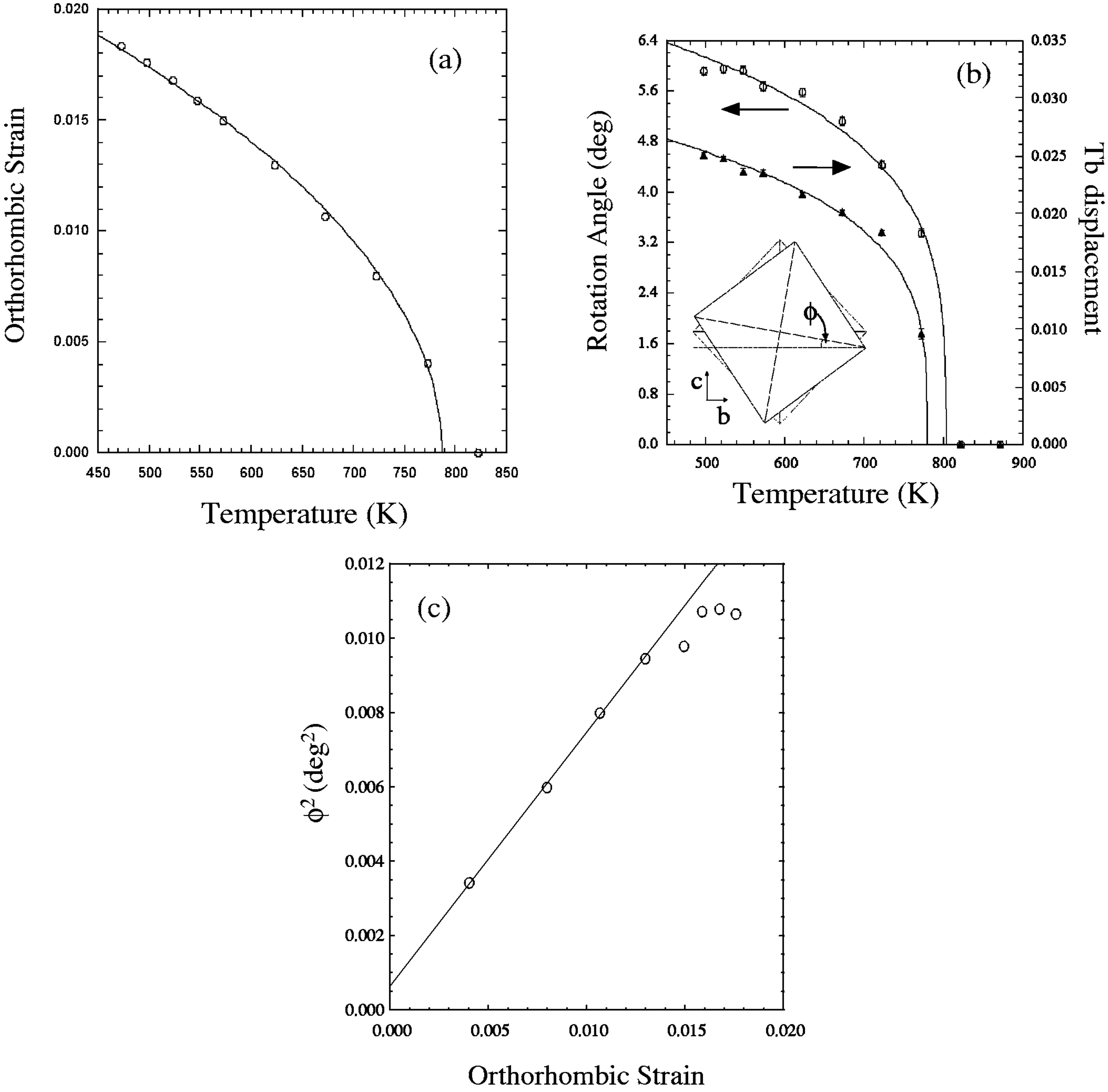

FIG. 5. Critical variations for the *Cmmm* to $P4/mmm$ structural phase transition in $TbBaMn_2O_6$. (a) Temperature dependence of the orthorhombic strain fitted as $o = o_0(1-T/T_0)^{1/2}$. (b) Temperature dependence of the octahedral rotation angle ϕ (open circles; inset diagram defines ϕ) and Tb displacements along the *a* axis (triangles) in $TbBaMn_2O_6$. Both variables are fitted by critical functions $Q = Q_0(1-T/T_0)^{1/4}$. (c) Variation of ϕ^2 with o showing a linear fit to the first four points.

the low symmetry structure, and is associated with an instability at the S-point of the Brillouin zone boundary for the $P4/mmm$ structure. Such a zone-boundary instability imposes coupling constraints between the spontaneous strain below the phase transition, o, and the order parameter, Q, such that $o \propto Q^2$, and thus $o = o_0(1-T/T_0)^{2\beta}$. Taking this measured orthorhombicity as the square of the order parameter for the orthorhombic *Cmmm* to tetragonal $P4/mmm$ transition, a least-squares fit to the data of the form $o = o_0(1-T/T_0)^{1/2}$ can be obtained [Fig. 5(a)], implying $\beta = 1/4$. The excellent fit down to $T/T_0 = 0.6$, with a transition temperature $T_c = 514(1)$ °C, shows that the transition can be well-described by a tricritical Landau model. The transition is highly mean-field in character, therefore, which is likely to be a consequence of the relatively large spontaneous strain that develops below T_c and the associated long-range strain interaction.

The $P4/mmm$ to *Cmmm* transition involves an out-of-phase rotation of MnO_6 octahedra about the crystallographic *a* axis. The rotation angles can be estimated from the displacements of the oxygens in the *bc* plane away from their ideal tetragonal geometry coordinates and their temperature

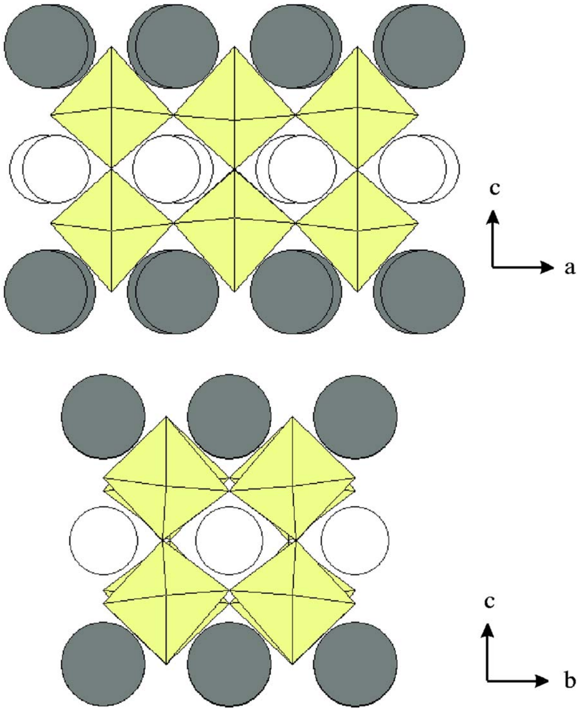

FIG. 6. (Color online) [100] and [010] projections of the 250 °C *Cmmm* structure of $TbBaMn_2O_6$, showing the *a*-axis tilts and the alternating short and long Tb—Tb separations along the *a* axis, respectively.

dependence is shown in Fig. 5(b). There is also a significant displacement of the terbium positions in the *Cmmm* structure from their ideal higher symmetry values [Fig. 5(b)], creating short and long Tb—Tb distances along the *a* direction. These displacements of the Tb cations from their ideal sites may drive the rotations as the octahedra shift to move the planar oxygen atoms away from the short Tb—Tb distance towards the longer, thereby optimizing the Tb—O separations (Fig. 6). The octahedral rotation angles, ϕ, and Tb separations, δx, clearly show a strong correlation. The $P4/mmm$ to *Cmmm* transition is typical of continuous structural transitions at which one or more of the cell parameters are doubled. For these transitions, the order parameter Q is initially proportional to the internal displacements such as ϕ or δx. This is verified by the fits of ϕ (or δx) $=\phi_0$ (or $\delta x_0)\cdot(1-T/T_0)^{1/4}$ to the data in Fig. 5(b). ϕ^2 varies linearly with orthorhombicity up to $o=0.013$ [Fig. 5(c)] beyond which higher order coupling terms become significant.

D. Differential scanning calorimetry

Differential scanning calorimetry of $TbBaMn_2O_6$ in the temperature regions surrounding the charge and orbital ordering transitions (Fig. 7) shows a very small step in the heat capacity ($\Delta C_p \approx 0.4\ \mathrm{J\ mol^{-1}\ K^{-1}}$) at 94.5 °C corresponding to the orbital ordering transition, and a larger discontinuity (indicative of first-order behavior, with $\Delta C_p \approx 20\ \mathrm{J\ mol^{-1}\ K^{-1}}$) at an onset temperature of 201 °C corresponding to the charge ordering transition. Both transition temperatures are consistent with the results of the neutron diffraction study. The excess entropy associated with the 201 °C heat capacity anomaly is $2.45\ \mathrm{J\ mol^{-1}}$ when integrated over the region within 40 K of the transition. The heat effects associated with the displacive and continuous orthorhombic-tetragonal phase transition at 514 °C were not sufficiently significant to be detectable in this region, which suffers from greater baseline drift and noise in the calorimeter.

IV. $YBaMn_2O_6$

A. Phase transitions

As reported previously,[7] $YBaMn_2O_6$ shows no *b*-doubled superstructure peaks down to 4 K. The room temperature diffraction pattern is instead characterized by the strong superstructure reflections at ~2.3 Å, a large monoclinic splitting of the intense (202) reflection and a subtle splitting of the (220) reflection which evidences a descent to a triclinic $P\bar{1}$ symmetry. This FOO phase persists in $YBaMn_2O_6$ up to 200 °C (Table IV).

At 225 °C a phase transition occurs, above which the triclinic splitting of the (220) reflection is no longer observed. However, the (202) peak is split above the transition (Fig. 8) whereas a single peak is expected for the *Cmmm* phase found above the charge ordering transition in $TbBaMn_2O_6$. This shows that the symmetry of the high-temperature $YBaMn_2O_6$ phase is lower than orthorhombic,

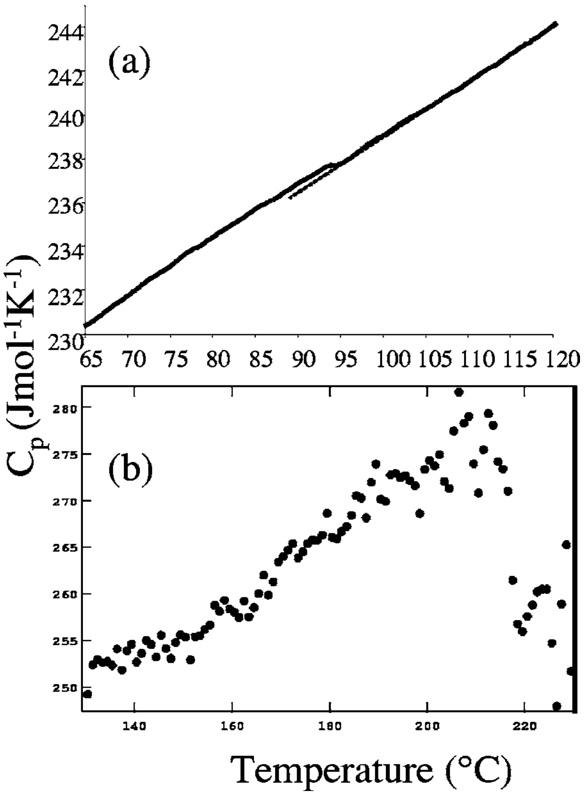

FIG. 7. Heat capacity, C_p, variations for $TbBaMn_2O_6$ from the DSC experiments. (a) Between 65 and 120 °C—the small step at 94.5 °C signifies the second-order orbital ordering transition. (b) Between 120 and 260 °C, evidencing a first-order discontinuity in C_p at the 201 °C charge ordering transition.

and all the peaks are successfully indexed by a monoclinic *C*2/*m* cell. At 225 °C, a phase separation is observed, with reflections corresponding to both triclinic $P\bar{1}$ and monoclinic *C*2/*m* phases.

Between 400 and 450 °C, the splitting of the (202) peak is lost signifying another phase transition. Orthorhombic *Cmmm* symmetry is observed at 450 and 500 °C, as found in the analogous phase of $TbBaMn_2O_6$.

B. Structural models

1. $P\bar{1}$ phase

All of the $YBaMn_2O_6$ patterns between 100 and 200 °C were fitted well by a triclinic $P\bar{1}$ symmetry model [Fig. 9(a); see Table IV for all lattice parameters], as previously reported for the room temperature structure.[7] The atomic coordinates and lattice parameters were all freely refined. The distortions of the MnO_6 polyhedra in the triclinic $P\bar{1}$ phase evidence the rocksalt charge ordering of Mn^{3+} and Mn^{4+} up to approximately 225 °C (Table V; Fig. 10), although the difference in average Mn—O bond length of the two manganese sites is less than at room temperature. One *trans* pair of Mn—O bonds in the *xy* plane around the Mn^{3+} site is significantly longer than the other, suggesting that the ferro-type orbital order in $YBaMn_2O_6$ is maintained until the loss of charge ordering at 225 °C.

2. *C*2/*m* phase

This high-temperature phase was reported to have a triclinic $P\bar{1}$ structure,[5] however, fits to our highly resolved neutron data showed that excellent fits can be obtained using the higher monoclinic *C*2/*m* symmetry [Fig. 9(c)] with no evidence for distortions to lower symmetry. Only one type of Mn site is present and no charge or orbital ordering distortions are observed in the *C*2/*m* phase. The 225 °C *C*2/*m* to $P\bar{1}$ transition therefore represents both the charge and orbital ordering transition in $YBaMn_2O_6$. The diffraction profile at 225 °C is well-described by a mixture of triclinic $P\bar{1}$ and

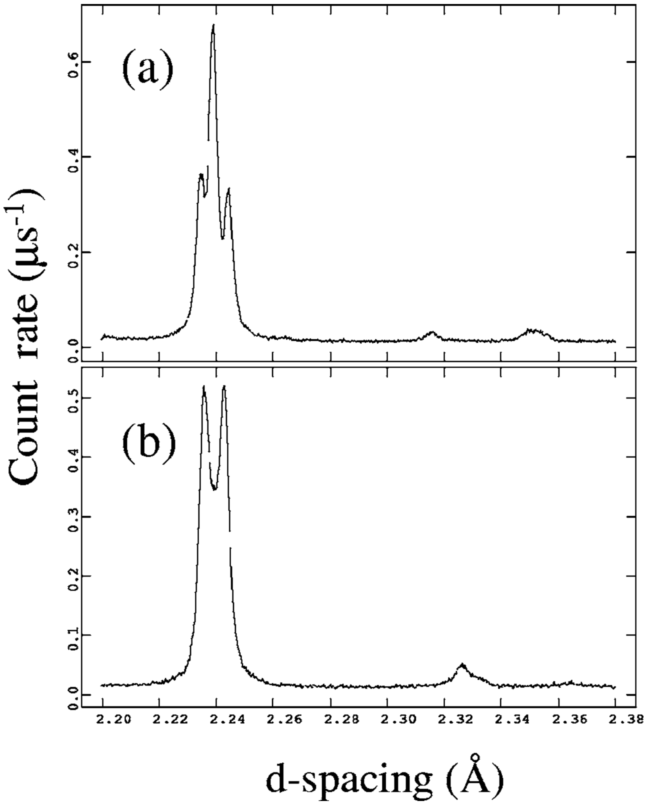

FIG. 8. Part of the backscattering detector diffraction data for $YBaMn_2O_6$ at (a) 200 °C and (b) 250 °C. The change in splitting of the (202) reflection at 2.24 Å reveals the change from the charged ordered $P\bar{1}$ phase to the *C*2/*m* structure.

TABLE IV. Thermal evolution of the space group symmetry and lattice parameters of $YBaMn_2O_6$

Temp (°C)	Space group	*a* (Å)	*b* (Å)	*c* (Å)	*α* (deg.)	*β* (deg.)	*γ* (deg.)
100	$P\bar{1}$	5.52015(7)	5.51503(7)	7.61501(9)	90.009(2)	90.274(1)	90.104(1)
125	$P\bar{1}$	5.51958(7)	5.51515(7)	7.62169(9)	90.014(2)	90.268(1)	90.108(1)
150	$P\bar{1}$	5.51911(7)	5.51516(7)	7.62745(8)	90.012(2)	90.265(1)	90.102(1)
175	$P\bar{1}$	5.51775(7)	5.51479(7)	7.63399(9)	90.010(2)	90.260(1)	90.104(1)
200	$P\bar{1}$	5.51615(5)	5.51393(7)	7.64151(9)	90.012(2)	90.253(1)	90.106(1)
225	$P\bar{1}$	5.5155(4)	5.5126(4)	7.6452(2)	90.010(8)	90.154(6)	90.095(4)
225	*C*2/*m*	7.8582(1)	7.6778(1)	7.7018(1)		90.240(1)	
250	*C*2/*m*	7.8546(1)	7.6832(1)	7.7056(1)		90.228(1)	
275	*C*2/*m*	7.8509(1)	7.6892(1)	7.7095(1)		90.225(1)	
300	*C*2/*m*	7.8470(1)	7.6958(1)	7.7139(1)		90.214(1)	
350	*C*2/*m*	7.8381(1)	7.7104(1)	7.7224(1)		90.182(1)	
400	*C*2/*m*	7.8275(1)	7.7308(2)	7.7294(2)		90.093(2)	
450	*Cmmm*	7.8121(1)	7.7578(1)	7.7366(1)			
500	*Cmmm*	7.7997(1)	7.7825(1)	7.7437(1)			

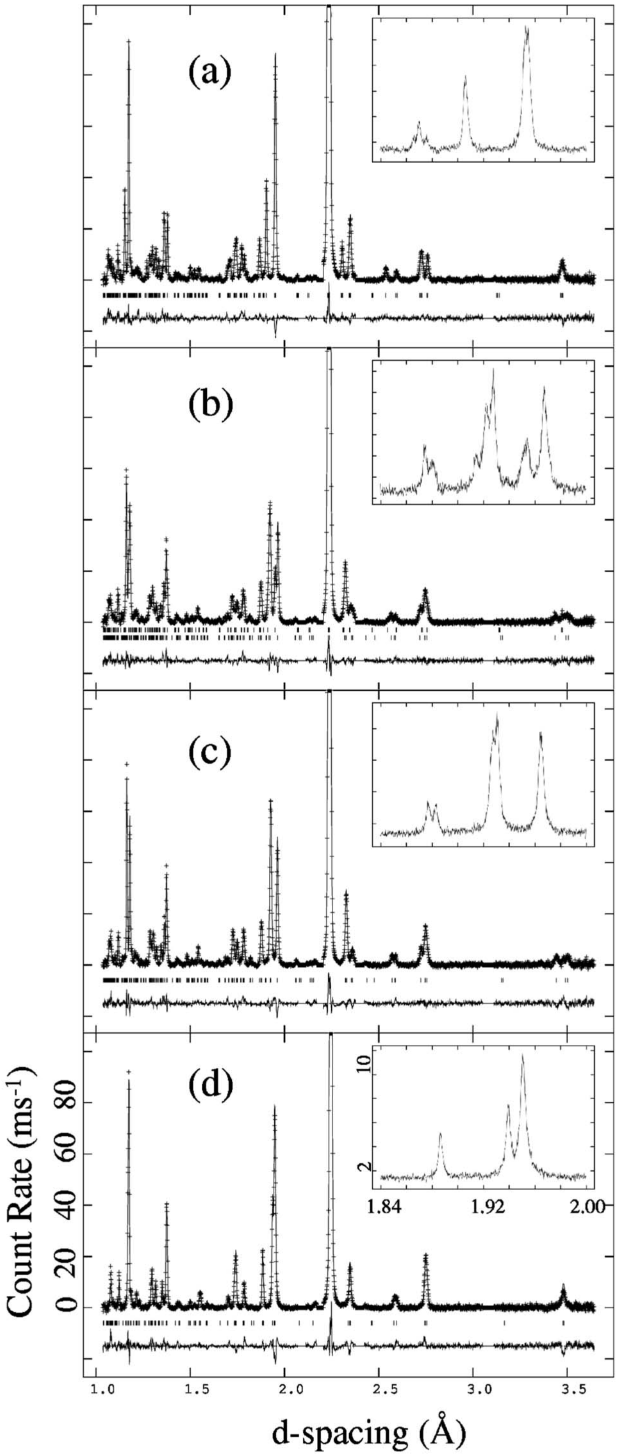

FIG. 9. Powder neutron diffraction profiles from the $2\theta=90°$ HRPD detector for YBaMn$_2$O$_6$ at representative temperatures. (a) 100 °C fitted in triclinic space group $P\bar{1}$. (b) 225 °C fitted as a mixture of triclinic $P\bar{1}$ and $C2/m$ phases. (c) 300 °C fitted in monoclinic space group $C2/m$. (d) 500 °C fitted in orthorhombic space group *Cmmm*. The intense (202) reflection at 2.2 Å has a peak count rate of 490 ms^{-1}, but the vertical scale has been truncated to enable other peaks to be seen clearly. The inset regions show the sensitivity of the backscattering detector data to the changes of symmetry and phase coexistence in (b).

monoclinic $C2/m$ phases [Fig. 9(b)] showing a small phase coexistence region around the first-order CO transition.

3. Cmmm phase

The diffraction patterns at 450 and 500 °C were fitted well by an orthorhombic *Cmmm* symmetry model [Fig. 9(d)]. No coherent distortions of the single MnO$_6$ polyhedra are observed in this *Cmmm* phase. It is neither charge nor orbitally ordered at these temperatures, and is distinguished from the monoclinic $C2/m$ phase only by the loss of some octahedral tilts as described later.

C. Critical variations

The refined cell parameters in YBaMn$_2$O$_6$ show a similar behavior to those in the terbium analog, with a general steady increase interrupted by a strong discontinuity at the CO transition from triclinic $P\bar{1}$ to monoclinic $C2/m$ phases, and an accompanying change in the slope of the cell volume (Figs. 11 and 12). The structural refinements described above show the presence of two high-temperature phase transitions in YBaMn$_2$O$_6$ between room temperature and 500 °C—a charge ordering transition at $T_{\mathrm{CO}}\approx 225$ °C and a structural transition at ≈400 °C. The discontinuity in the cell parameters, coupled with the phase coexistence observed at the charge ordering transition are clearly indicative of it being first order, whereas the continuous variation of the cell parameters through the $C2/m$ to *Cmmm* transition strongly suggest it to be second order. The transition from *Cmmm* to the aristotype $P4/mmm$ tetragonal structure was not observed up to the maximum experimental temperature of 500 °C, but from the convergence of a and b cell parameters (Fig. 11), we estimate that the transition occurs at 525–550 °C

The macroscopic strains in the $C2/m$ monoclinic phase can be characterized by the monoclinic angle, β. The *Cmmm* to $C2/m$ transition is a zone-center instability, with both structures having a $2\times2\times2$ superlattice with respect to the cubic $Pm\bar{3}m$ perovskite structure. In order to determine whether the monoclinic to orthorhombic transition is in accordance with Landau theory, we therefore take the appropriate component of the spontaneous strain tensor[12] to be proportional to the order parameter, Q, this component corresponding to the strain induced by the angular distortion of the *ac* plane. For a monoclinic-orthorhombic transition, we can then approximate this strain as being proportional to $-\cos\beta$. The temperature dependence of $-\cos\beta$ is shown in Fig. 13, with a fit of $-\cos\beta=-\cos\beta_0(1-T/T_0)^{1/2}$. This fits the data moderately well, suggesting that this second-order transition can be described by a second-order Landau model, and gives a transition temperature of 437(13) °C.

The monoclinic $C2/m$ phase of YBaMn$_2$O$_6$ involves two independent out-of-phase rotations, about the crystallographic a and c axes. The a-axis rotation is analogous to that observed in the *Cmmm* phase of TbBaMn$_2$O$_6$ and its magnitude can be estimated in the same way from the oxygen coordinates. It correlates strongly with the Y—Y separation along the a axis, suggesting an equivalent driving force to

TABLE V. Manganese-oxygen distances (Å) in the $YBaMn_2O_6$ structures.

		Mn1-O						Mn2-O							
Temp (°C)	Space group	Mn1-O1(a)	Mn1-O2	Mn1-O3	Mn1-O4(a)	Mn1-O1(b)	Mn1-O4(b)	Mn2-O1(a)	Mn2-O2	Mn2-O3	Mn2-O4(a)	Mn2-O1(b)	Mn2-O4(b)	⟨Mn1-O⟩	⟨Mn2-O⟩
100	$P\bar{1}$	1.964(8)	1.996(9)	1.887(8)	1.943(8)	2.007(8)	2.013(8)	2.003(7)	1.915(9)	1.904(8)	1.960(7)	1.980(9)	1.873(9)	1.968(8)	1.939(8)
125	$P\bar{1}$	1.959(8)	1.989(9)	1.906(8)	1.952(8)	1.971(8)	2.008(8)	1.984(7)	1.915(9)	1.901(8)	1.972(7)	2.006(9)	1.888(8)	1.964(8)	1.944(8)
150	$P\bar{1}$	1.962(7)	2.005(8)	1.900(7)	1.945(8)	1.995(8)	2.005(8)	1.993(7)	1.912(8)	1.899(7)	1.965(7)	1.980(8)	1.890(8)	1.969(8)	1.940(8)
175	$P\bar{1}$	1.961(8)	2.005(8)	1.907(7)	1.942(8)	1.989(8)	1.997(8)	2.001(7)	1.912(8)	1.896(7)	1.956(7)	1.984(9)	1.897(9)	1.967(8)	1.941(8)
200	$P\bar{1}$	1.948(8)	2.012(8)	1.914(7)	1.939(8)	1.991(8)	1.979(9)	2.006(8)	1.914(9)	1.887(7)	1.960(8)	1.979(9)	1.916(9)	1.964(8)	1.944(9)
		Mn—O													
		Mn—O1	Mn—O2	Mn—O3	Mn—O4	Mn—O5	Mn—O5	⟨Mn—O⟩							
250	$C2/m$	1.913(1)	1.974(1)	1.970(3)	1.915(3)	1.935(3)	2.018(3)	1.948(1)							
275	$C2/m$	1.911(1)	1.978(1)	1.970(2)	1.917(2)	1.925(3)	2.025(3)	1.949(1)							
300	$C2/m$	1.914(1)	1.975(1)	1.975(2)	1.916(2)	1.936(3)	2.014(3)	1.949(1)							
350	$C2/m$	1.919(1)	1.974(1)	1.980(2)	1.918(2)	1.905(3)	2.037(3)	1.950(1)							
400	$C2/m$	1.922(1)	1.971(1)	1.977(3)	1.930(3)	1.912(3)	2.024(3)	1.951(1)							
		Mn—O1	Mn—O2	Mn—O3	Mn—O4	Mn—O5 (×2)									
450	*Cmmm*	1.904(1)	1.979(1)	1.991(4)	1.918(4)	1.959(2)	1.952(1)								
500	*Cmmm*	1.910(1)	1.992(1)	2.012(4)	1.897(4)	1.957(3)	1.954(1)								

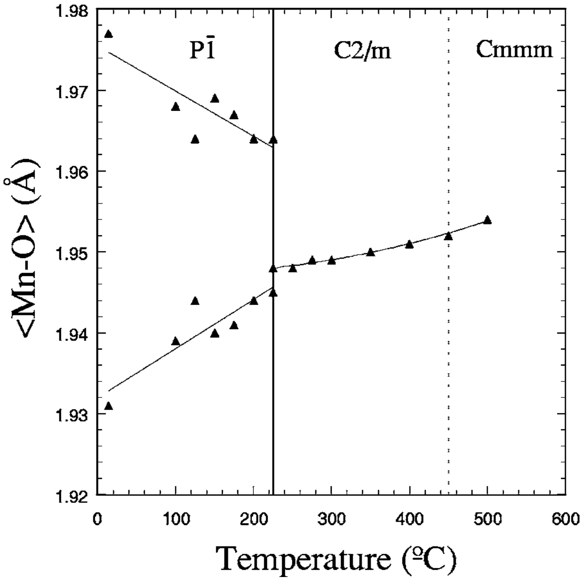

FIG. 10. Temperature dependence of the average Mn—O bond lengths in $YBaMn_2O_6$. Lower temperature $P\bar{1}$ structures contain two manganese sites, higher temperature structures only one. Solid/dashed vertical lines show the first/second-order phase transitions. Lines through points are guides to the eye.

that in $TbBaMn_2O_6$ (Fig. 14). The c-axis rotation angle can be estimated from the atomic positions in an analogous manner, this time, however, using the movement of the oxygen atoms from their ideal tetragonal coordinates in the ab-plane. The temperature dependence again correlates with the Y displacements, this time in the z direction. Fits to ϕ and δz, of the form $A(1-T/T_0)^n$, were attempted to describe the c-axis rotation in $YBaMn_2O_6$, but they gave a poor agreement, and yielded wildly differing transition temperatures. The inability to fit these functions with a simple Landau-type second-order model suggests a strong coupling of these parameters to other structural degrees of freedom, and makes them only approximate order parameters for describing the monoclinic $C2/m$ to orthorhombic $Cmmm$ transition.

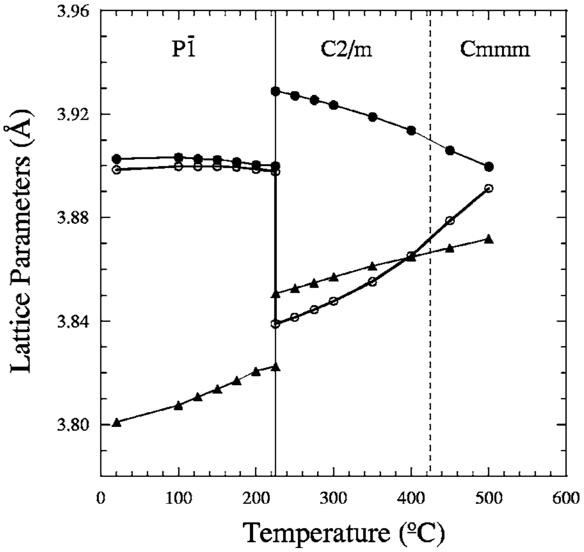

FIG. 11. Temperature dependence of the pseudo-cubic a (closed circles), b (open circles), and c (triangles) lattice parameters of $YBaMn_2O_6$. Solid/dashed vertical lines show the first/second-order phase transitions.

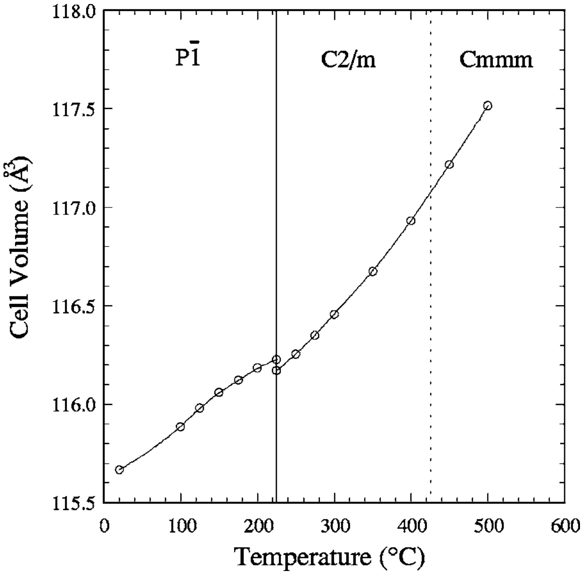

FIG. 12. Temperature dependence of cell volume of $YBaMn_2O_6$. Solid/dashed vertical lines show the first/second-order phase transitions. Lines through points are a guide to the eye.

V. DISCUSSION

The small size difference between Tb^{3+} and Y^{3+} gives rise to significant differences in the ordering of charge, orbital, and octahedral tilt states in their $RBaMn_2O_6$ materials. The results of this high temperature study are summarized in Fig. 15. The room temperature orderings of the two phases were previously known to be different. $TbBaMn_2O_6$ has a $\sqrt{2}a_p \times 2\sqrt{2}a_p \times 2a_p$ triclinic superstructure which is charge

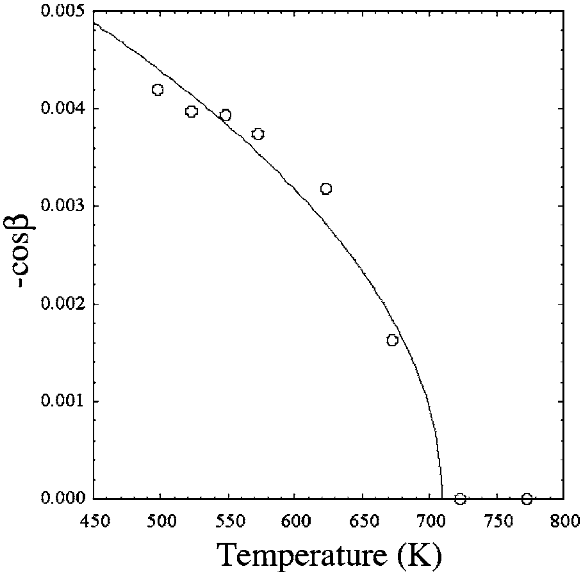

FIG. 13. Critical variation of the monoclinic strain $-\cos\beta$ at the $C2/m$ to $Cmmm$ phase transition of $YBaMn_2O_6$, fitted as $-\cos\beta = -\cos\beta_0(1-T/T_0)^{1/2}$.

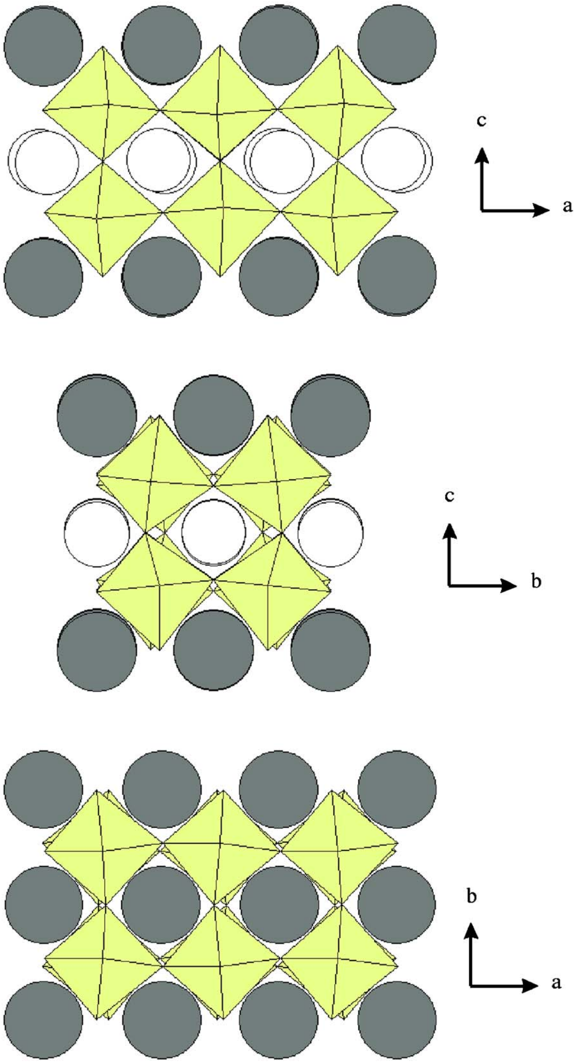

FIG. 14. (Color online) [001], [100], and [010] projections of the $C2/m$ structure of $YBaMn_2O_6$ at 300 °C, illustrating the c-axis tilting, the a-axis tilting, and the alternating Y displacements, respectively.

and antiferro-orbitally ordered,[6] whereas $YBaMn_2O_6$ has a charge and ferro-orbitally ordered $\sqrt{2}a_p \times \sqrt{2}a_p \times 2a_p$ cell that also has triclinic $P\bar{1}$ symmetry.[7] The degree of charge ordering, estimated from the Mn—O bond distances (Figs. 2 and 10) reaches a maximum of 45% and 60%, for $YBaMn_2O_6$ and $TbBaMn_2O_6$, respectively, of the ideal Mn^{3+}/Mn^{4+} separation. This reduced magnitude is typical for symmetry-broken charge-ordered transition metal oxide structures, as discussed previously.[6,7]

This study shows that the ambient temperature $YBaMn_2O_6$ structure remains up to $T_{CO} = 225$ °C. However, $TbBaMn_2O_6$ transforms to another charge ordered $\sqrt{2}a_p \times \sqrt{2}a_p \times 2a_p$ structure at 94.5 °C and this phase persists up to the 200 °C charge ordering transition. Whether this CO phase of $TbBaMn_2O_6$ has monoclinic $P2_1/m$ symmetry and is orbitally disordered, or has a triclinic ferro-orbital ordered structure like the $P\bar{1}$ phase of $YBaMn_2O_6$ is not clear from our neutron diffraction data. The triclinic distortion in $YBaMn_2O_6$ is close to the resolution limit of HRPD, and any FOO lattice distortion in $TbBaMn_2O_6$ will be even smaller.

The two scenarios for the evolution of $TbBaMn_2O_6$ up to T_{CO} can be distinguished using the DSC results. If the 94.5 °C transition corresponds to a loss of Mn^{3+} orbital ordering then the transition should be first order with an ideal statistical entropy contribution of $R \ln 2$, as the orbital distortions have two possible directions in the ab-plane. A further $R \ln 2$ entropy change should be seen at the 200 °C charge ordering transition, as there are two arrangements for the Mn^{3+}/Mn^{4+} CO. Hence two first-order transitions with comparable transition entropies are expected. In the second scenario, the AFOO to FOO transformation at 94.5 °C has no statistical entropy change and so the transition can be continuous, while a large entropy release (ideally $2R \ln 2$) is expected when both CO and FOO are lost at 200 °C. The observed data (Fig. 7) support the second scenario, with a very small heat capacity change of $\Delta C_p \approx 0.4$ J/mol/K at 94.5 °C and a larger heat effect with a first-order jump of $\Delta C_p \approx 20$ J/mol/K at 200 °C. However, the integrated excess entropy of 2.45 J mol^{-1} is somewhat smaller than the statistical estimate of $2R \ln 2$ (11.5 J mol^{-1}) showing that significant charge and orbital correlations persist above T_{CO}.

From comparison of the heat capacity anomalies at the two transitions, we conclude that the "$P2_1/m$" phase of $TbBaMn_2O_6$ is ferro-orbitally ordered like the analagous $YBaMn_2O_6$ phase. This conclusion is corroborated by the similarity of T_{CO}'s for $TbBaMn_2O_6$ (200 °C) and $YBaMn_2O_6$ (225 °C) suggesting that the orderings below

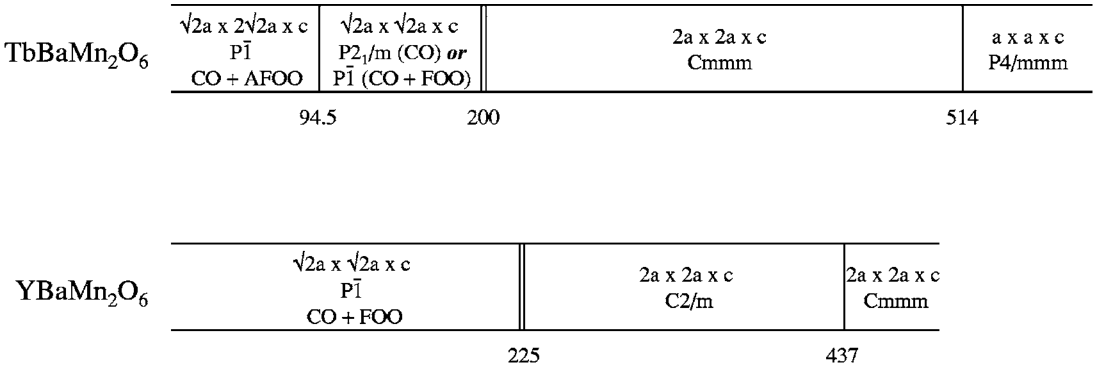

FIG. 15. Summary figure to illustrate the phase changes with temperature (°C) for $TbBaMn_2O_6$ and $YBaMn_2O_6$. Single vertical lines represent second-order phase transitions, double lines represent first-order transitions with observed phase coexistence.

the transition are the same in both materials. The 94.5 °C transition between charge ordered, antiferro- and ferro-orbitally ordered phases in $TbBaMn_2O_6$ is not reported in other manganites, and shows that multiple orbital ordering degrees of freedom are available even when the charge ordering is fixed.

The charge ordering transitions of 473 and 498 K, respectively, for $TbBaMn_2O_6$ and $YBaMn_2O_6$ are high compared to those of ~200 K in conventional half-doped manganites without A-site cation order, although charge ordering temperatures of 475 K have previously been reported for the $(Bi,Sr)MnO_3$ (Refs. 13 and 14) system. The robustness of Mn^{3+}/Mn^{4+} charge ordering in $RBaMn_2O_6$ is most likely due to the large internal strains imposed by the A cation order of the small Tb^{3+} and large Ba^{2+} in alternating layers. The volume (V) decrease and increase in volume expansion (dV/dT) on warming through the transition are typical for charge ordering (insulator to metal) transitions. The volume decrease results from the change in electron kinetic energy and vibrationally assisted (polaronic) conduction above the transition leads to the increase in dV/dT.

Phase coexistence is observed below T_{CO} down to lowest temperatures in conventional manganites, and the microstructures of ferromagnetic, noncharge ordered, and insulating charge ordered regions give rise to notable physical properties such as CMR. In the $RBaMn_2O_6$ phases we observe a small two phase region, <50 K wide in both materials, in keeping with the first order nature of the structural transition between nonisomorphous space group symmetries. A previous study of $YBaMn_2O_6$ using high-temperature magnetic susceptibility, electrical resistivity, and calorimetry measurements[5] reported that two phase transitions were present, at 480 and 520 K. However, our results suggest that these are the limits of the coexistence region around a single charge ordering transition. The difference between the phase coexistence behaviors of A-site ordered and disordered manganites may result from the different magnitudes of their transition temperatures. At ~200 K, there is not enough thermal energy to anneal out the strains between the two phases and fully transform to the low temperature charge ordered phase in conventional manganites, whereas at ~500 K the transformation is completed in the $RBaMn_2O_6$ materials. In general, such first-order transitions occur because the dominant structural instabilities in manganites are for ordering octahedral tilts and rotations at high temperatures. Charge ordering occurs at lower temperatures in structures that already have tilts or rotations ordered with an incompatible symmetry, and so the transition is first order.

Above T_{CO}, there is no long range order of Mn charge or orbital states in the $RBaMn_2O_6$ materials, but superstructures are still observed through ordering of tilts or rotations of the MnO_6 octahedra. Such superstructures are ubiquitous in conventional ABO_3 perovskites and the symmetry relations between the ordered phases are much studied. A group theoretical analysis for tilt orderings in A-site ordered perovskites has been reported recently.[11] We find that the favored distortion from the aristotype $P4/mmm$ symmetry of $RBaMn_2O_6$ is to the $Cmmm$ superstructure in which out-of-phase rotations of the octahedra around the a axis are ordered. The ordering is described well by a mean field approximation to Landau theory. A second symmetry-breaking distortion to monoclinic $C2/m$ is observed for small R=Y (but not R=Tb) in which additional rotations around c are ordered.

In summary, successive orderings on cooling of MnO_6 octahedral rotations, Mn^{3+}/Mn^{4+} charges, Mn^{3+} orbital states (and Mn spin states at lower temperatures) lead to a rich variety of superstructures and physical states in $RBaMn_2O_6$ manganites. The A-cation ordering in these phases leads to significantly different properties than conventional half-doped manganites. An alternative (rock salt) charge ordering occurs at much higher temperatures, and with a more limited phase coexistence region. $TbBaMn_2O_6$ shows an unprecedented antiferro- to ferro-orbital order transition within the charge ordered regime.

ACKNOWLEDGMENTS

The authors thank Dr. Richard Ibberson, Jan-Willem Bos, and Falak Sher for their assistance with collection of the neutron data and EPSRC for provision of neutron beam time. A.J.W. acknowledges EPSRC and the Rutherford-Appleton Laboratory for support.

---

[1] F. Millange, E. Suard, V. Caignaert, and B. Raveau, Mater. Res. Bull. **34**, 1 (1999).

[2] F. Millange, V. Caignaert, B. Domenges, B. Raveau, and E. Suard, Chem. Mater. **10**, 1974 (1998).

[3] T. Nakajima, H. Kageyama, H. Yoshizawa, and Y. Ueda, J. Phys. Soc. Jpn. **71**, 2843 (2002).

[4] T. Arima, D. Akahoshi, K. Oikawa, T. Kamiyama, M. Uchida, Y. Matsui, and Y. Tokura, Phys. Rev. B **66**, 140408(R) (2002).

[5] T. Nakajima, H. Kageyama, M. Ichihara, K. Ohoyama, H. Yoshizawa, and Y. Ueda, J. Solid State Chem. **177**, 987 (2004).

[6] A. J. Williams and J. P. Attfield, Phys. Rev. B **66**, 220405(R) (2002).

[7] A. J. Williams and J. P. Attfield, Phys. Rev. B **72**, 024436 (2005).

[8] P. G. Radaelli, D. E. Cox, M. Marezio, and S.-W. Cheong, Phys. Rev. B **55**, 3015 (1997).

[9] A. C. Larson and R. B. Von Dreele, General Structure Analysis System (GSAS) Report No. LAUR 86–748, Los Alamos National Laboratory, 1994 (unpublished).

[10] C. Perca, L. Pinsard-Gaudart, A. Daoud-Aladine, M. T. Fernandez-Diaz, and J. Rodriguez-Carvajal, Chem. Mater. **17**, 1835 (2005).

[11] C. J. Howard and Z. Zhang, J. Phys.: Condens. Matter **15**, 4543 (2003).

[12] D. R. Pederzolli, G. M. Wltschek, J. P. Attfield, and H. Fuess, Phys. Rev. B **58**, 5226 (1998).

[13] C. Frontera, J. L. Garcia-Munoz, A. Llobet, M. A. G. Aranda, C. Ritter, M. Respaud, and J. Vanacken, J. Phys.: Condens. Matter **13**, 1071 (2001).

[14] J. L. Garcia-Munoz, C. Frontera, M. A. G. Aranda, A. Llobet, and C. Ritter, Phys. Rev. B **63**, 064415 (2001).